# Electrohydrodynamic Quincke rotation of a prolate ellipsoid

Quentin Brosseau, Gregory Hickey, and Petia M. Vlahovska

*School of Engineering, Brown University, Providence, Rhode Island 02912, USA*

(Received 6 September 2016; published 17 January 2017)

We study experimentally the occurrence of spontaneous spinning (Quincke rotation) of an ellipsoid in a uniform direct current (dc) electric field. For an ellipsoid suspended in an unbounded fluid, we find two stable states characterized by the orientation of the ellipsoid long axis relative to the applied electric field: spinless (parallel) and spinning (perpendicular). The phase diagram of ellipsoid behavior as a function of field strength and aspect ratio is in close agreement with the theory of Cēbers *et al.* [Phys. Rev. E **63**, 016301 (2000)]. We also investigate the dynamics of the ellipsoidal Quincke rotor resting on a planar surface with normal perpendicular to the field direction. We find behaviors, such as swinging (long axis oscillating around the applied field direction) and tumbling, due to the confinement.

## I. INTRODUCTION

The spontaneous spinning of a dielectric sphere in a uniform dc electric field has been known for over a century, first attributed to the work of Quincke [1]. This phenomenon is enjoying resurgent interest driven by the experimentally observed intriguing dynamics of Quincke-rotating spheres [2–5] and drops [6–11], as well as an increasing interest in electric field directed assembly of colloidal particles [12–15]. Theoretical analyses of rigid spheres show that an isolated sphere can exhibit Lorenz chaotic rotations [3], pairs of spheres can undergo intricate trajectories [16–18], large populations can self-organize and undergo directed motion [5,19–21], and a suspension can exhibit lower effective viscosity [22–24] or increased conductivity [25] compared to the suspending fluid.

The Quincke rotation is driven by misalignment of the particle induced-charge dipole and the applied electric field. When a particle is placed in an electric field, free charges accumulate at its interface due to the difference of electrical conductivity $\sigma$ and permittivity $\varepsilon$ between the particle $p$ and suspending $s$ medium [26],

$$R = \frac{\sigma_p}{\sigma_s}, \quad S = \frac{\varepsilon_p}{\varepsilon_s}. \tag{1}$$

A polarization corresponding to a dipole antiparallel to the applied electric field is unfavorable and can lead to rotation. The conditions for continuous rotation are determined from the analysis of the equations for free-charge polarization relaxation and conservation of angular momentum.

The evolution of the $i$th dipole component in a coordinate system centered at the particle [and in the case of an ellipsoid aligned with its axes (see Fig. 1)] is described by [27]

$$\frac{dP_i}{dt} = -\tau_i^{-1} \big[ P_i - \big( \chi_i^0 - \chi_i^\infty \big) E_i \big], \tag{2}$$

where $\chi_i^0$ and $\chi_i^\infty$ are the low- and high-frequency susceptibilities, respectively, and $\tau_i$ is the Maxwell-Wagner polarization time along the $i$th axis of the ellipsoid. The particle rotation with rate $\boldsymbol{\Omega}$ is described by

$$I_i \frac{d\Omega_i}{dt} = (\bar{\mathbf{P}} \times \mathbf{E})_i - \alpha_i \Omega_i, \tag{3}$$

where $I_i$ are the moments of inertia and $\alpha_i$ are the rotational friction coefficients around the $i$th axis. The electric torque is determined by the total polarization $\bar{P}_i = P_i + \chi_i^\infty E_i$.
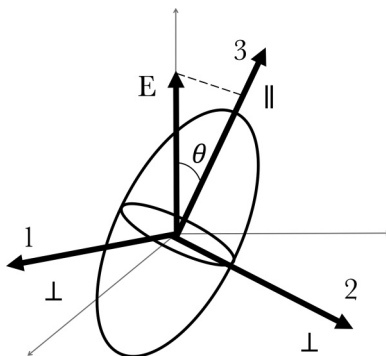
FIG. 1. Sketch of the problem.

For a shape-isotropic particle such as a sphere with radius $a$,

$$\chi^0 - \chi^\infty = 4\pi\varepsilon_s a^3 \frac{3(R-S)}{(R+2)(S+2)} \tag{4}$$

and the Maxwell-Wagner polarization time is

$$\tau_{\mathrm{MW}} = \frac{\varepsilon_p + 2\varepsilon_s}{\sigma_p + 2\sigma_s}. \tag{5}$$

Analysis of (2) and (3) shows that the sphere spins with constant rate around an axis perpendicular to the applied field direction [26,28,29] above a critical field strength $E > E_Q$,

$$E_Q^2 = -\frac{\alpha}{\tau_{\mathrm{MW}}(\chi^0 - \chi^\infty)} = \frac{2\sigma_s\mu_s(R+2)^2}{3\varepsilon_s^2(S-R)}, \tag{6}$$

where $\alpha = 8\pi\mu_s a^3$ is the rotational friction coefficient of the sphere. Equation (6) shows that the electrorotation is possible only if $\chi^0 - \chi^\infty < 0$, i.e., the suspending fluid and sphere satisfy the condition $R/S < 1$. Physically, this corresponds to the induced dipole moment of the sphere oriented opposite to the direction of the applied field. A perturbation in the dipole orientation produces torque, which induces physical rotation of the sphere (around an axis perpendicular to the applied field direction). The induced surface-charge distribution rotates with the sphere, however, the exterior fluid recharges the interface. The balance between charge convection by rotation and supply by conduction from the bulk results in a steady oblique orientation of the dipole relative to the field direction and constant torque.

An ellipsoidal particle is expected to display more complex electrorotation dynamics than a sphere [27,30–34] due to its anisotropic shape. The polarization relaxation times and susceptibilities along the long and short axes differ [see Eq. (A2)]. The classic result is that an axisymmetric ellipsoid aligns its long axis with the applied electric field [27,35]. In stronger fields, however, a stable orientation with the long axis perpendicular to the external dc field is predicted [27]. In this state, the prolate ellipsoid is rotating around its long axis (spinning state) [see Fig. 2(a) for an illustration]. The spinning state occurs above a threshold [27]

$$E_a^2 = -\frac{\alpha_\parallel}{\tau_\perp(\chi_\perp^0 - \chi_\perp^\infty)}, \tag{7}$$

where $\parallel$ denotes the ellipsoid symmetry (long) axis and $\perp$ the perpendicular-to-symmetry (short) axis. In addition, $\alpha_\parallel$ is the friction coefficient for rotation around the long axis given by (A7).
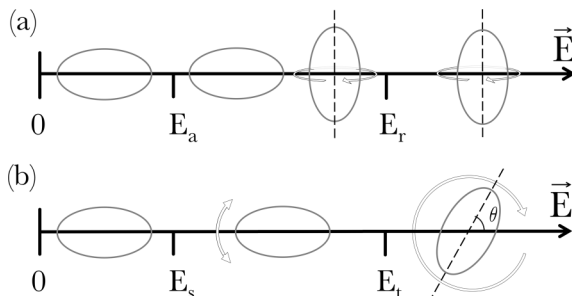
FIG. 2. Summary of prolate ellipsoid stable steady states and threshold electric fields. (a) Bulk, spinless parallel; $E > E_a$, coexistence of spinless parallel and spinning perpendicular; and $E > E_r$, spinning perpendicular. (b) Resting on a surface, spinless parallel; $E > E_s$, swinging; and $E > E_t$, tumbling.

For a certain range of electric field strengths the system is bistable, i.e., the two orientations, parallel and transversal to the applied field, coexist. The bistability disappears above $E > E_r$,

$$E_r^2 = \frac{\alpha_\perp}{\alpha_\parallel} E_a^2 \frac{\chi_\perp^\infty - \chi_\perp^0}{\chi_\perp^\infty - \chi_\parallel^0}. \tag{8}$$

At even higher field strengths, time integration of the equations of motion (3) and polarization relaxation (2) shows that the ellipsoid axis can begin to precess around the field direction; regimes of both regular and chaotic oscillations are found with increasing field strength [36–38]. These theoretically predicted peculiar features of the electrorotation of ellipsoids have not been experimentally verified and motivate our work. In this paper we perform a systematic study of ellipsoid dynamics as a function of field strength and aspect ratio for a prolate ellipsoid.

## II. EXPERIMENTAL METHODS

### A. Preparation of the ellipsoid

The millimeter-sized ellipsoid, needed for direct visualization, is made by cross-linking a spheroidally deformed drop of polymer NOA 81 (Norland Optical Adhesive). The drop deformation is induced by application of a uniform dc electric field after the drop is suspended in poly(dimethyl)siloxane of viscosity 500 cSt (UCT) in a setup similar to that in [7,9]. Once steady-state deformation is reached, the drop is exposed to UV radiation of 365 nm for about 1 min. Aspect ratios ranging from 1 to 2 can be achieved by tuning the electric field strength from 0 to 5.0 kV/m. Once cross-linked, the solid NOA particles ($\varepsilon_p = 4.04\varepsilon_0$, $\sigma_p = 10^{-17}$ S/m, and density $\rho_p \sim 1.2$ g/cm$^3$) are rinsed and transferred to the castor oil bath ($\varepsilon_s = 4.8\varepsilon_0$, $\sigma_s = 4.4 \times 10^{-11}$ S/m, $\rho_s = 0.961$ g/cm$^3$, and viscosity $\mu_s = 0.69$ Pa s), where the experiments are performed.

### B. Experimental setup and procedure

A uniform electric field is generated in a parallel-plate chamber setup sketched in Fig. 3(a). The chamber base and walls are constructed from polymethyl methacrylate (PMMA). Two $4 \times 7$ cm$^2$ brass plates serving as electrodes are attached to the chamber's vertical walls. The distance between the electrodes is 1.64 cm, about 10 times larger than the particle radius, to minimize boundary effects. Fields up to 3.0 kV/cm are generated using a voltage amplifier connected to a dc power supply. The ellipsoid is observed from the top, in a direction perpendicular to the field.

The experiment is carried out by placing the solid NOA ellipsoid into the chamber filled with castor oil. The particle is placed either in the bulk (to observe unbounded dynamics) or at the bottom (to observe planar rotations). After the electric field is applied, the ellipsoid behavior is recorded
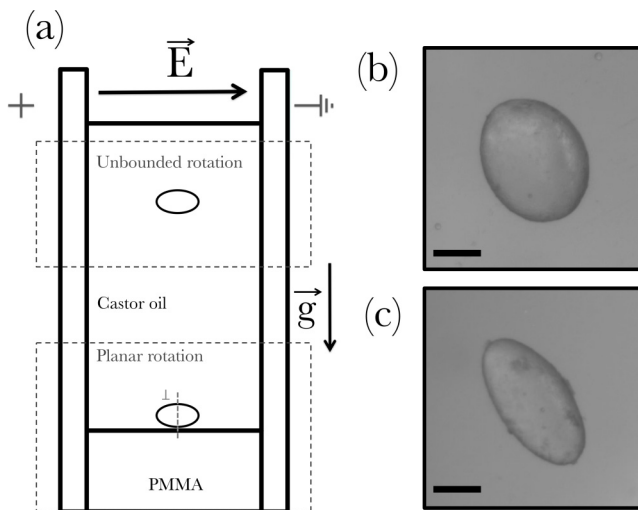
FIG. 3. (a) Sketch of the experimental setup. Rotation is observed either an ellipsoid in the bulk or an ellipsoid resting on a horizontal PMMA surface. The top view of two NOA ellipsoids is shown with aspect ratio (b) $\beta = 1.25$ and (c) $\beta = 1.93$. The scale bar is 500 $\mu$m.

for about 3 min. This time limit is set by particle sedimentation (with velocity of about 0.4 mm/s). For a given electric field, the experiment is repeated 2–10 times for the same particle with different initial orientation between the ellipsoid long axis and the applied field direction. The same steady state is always observed. After a series of experiments in the bulk, the planar rotations of the same particle are studied after it reaches the bottom of the chamber.

The motion of the particle is recorded through an optical device mounted on top of the chamber. From the images the following parameters of interest are obtained: particle geometry (volume and aspect ratio $\beta = a_{\parallel}/a_{\perp}$) and the dynamic angle $\theta(t)$ between the particle symmetry (long) axis and the applied electric field $E$.

## III. RESULTS AND DISCUSSION

### A. Unbounded rotation

Figure 4(a) shows the steady states for ellipsoids in an unbounded environment as a function of field strength. Nine ellipsoids with aspect ratios between $\beta = 1.02$ and $\beta = 1.96$ are investigated. Each particle is subjected to a stepwise increase of the electric field. The appearance of the spinning perpendicular state occurs above a threshold electric field, which agrees well with the theoretical predictions $E_a$ (dashed line) [Eq. (7)]. The spinless parallel state is never observed above $E_r$ (solid line) [Eq. (8)], also in agreement with the theory [27].

In the theoretically predicted bistability region $E_a < E < E_r$, ellipsoids with both spinning and aligned orientation are found. However, we never observe bistability with the same ellipsoid. Experimentally we find that a given particle always assumes the same state (aligned or spinning), independent of the initial orientation; however, two nearly identical ellipsoids (with only a minute difference in aspect ratio) at the same electric field can assume different states. It is likely that small imperfections of the ellipsoids introduce bias in the choice of the steady state and suppress the bistability. We do see hysteresis in the transition between spinless and spinning states for the same particle, but the window of electric fields is much narrower than the theoretically predicted bistability region.

Our experiments also highlight the rich transient dynamics as a particle approaches its steady state. Various evolutions are shown in Fig. 4(b) for an ellipsoid with aspect ratio $\beta = 1.4$.
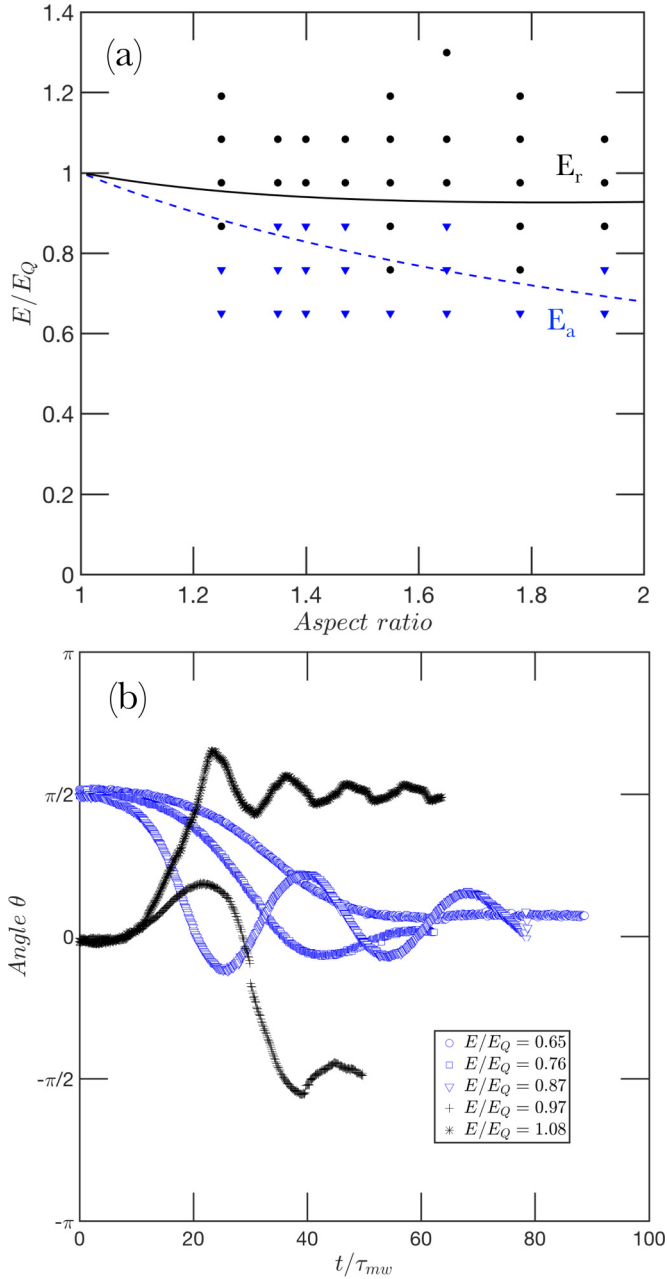
FIG. 4. (a) Phase diagram of unbounded dynamics of a prolate ellipsoid showing the two steady states: spinless parallel orientation (triangles) and spinning perpendicular (circles). Curves correspond to stability thresholds for the spinning perpendicular state $E_a$ [blue dashed line, Eq. (7)] and the loss of stability of the spinless parallel state $E_r$ [black solid line, Eq. (8)]. (b) Evolution of the ellipsoid orientation at $E < E_a$ (blue curve) and $E > E_r$. The corresponding initial orientations $\theta = \pi/2$ and 0 are chosen to be as far away as possible from the steady orientation. The aspect ratio $\beta = 1.4$.

If the applied field is $E < E_a$, the particle is initially placed out of equilibrium with its long axis perpendicular to the field direction [$\theta(t = 0) = \pi/2$; this corresponds to a maximum deviation from

the steady state $\theta_{eq} = 0$. When the field is turned on, the spinless state is reached monotonically at low field strengths. In stronger fields, the steady orientation is approached via damped oscillations around the parallel orientation.

If the applied field is $E > E_a$, the particle is again placed out of equilibrium, initially in parallel alignment [$\theta(t = 0) = 0$], and its relaxation towards the spinning perpendicular orientation $\theta_{eq} = \pi/2$ is recorded. Here again two possible relaxation behaviors exist. Slightly above the threshold value $E_r$ [Fig. 4(b)], the long axis exhibits growing oscillations until the onset of the spinning motion stabilizes the orientation at $\theta_{eq} = \pi/2$ [30]. If the particle initial orientation is the equilibrium one $\theta(t = 0) = \pi/2$, then spinning takes place immediately and this initial orientation is maintained (see Supplemental Material Ref. [39]). In the spinning regime oscillations around $\theta = \pi/2$ are sometimes observed [see Fig. 3(b), where $E/E_Q = 1.08$] that correspond to out-of-plane precession of the symmetry axis.

## B. Planar rotations

In this section we consider the dynamics of a prolate ellipsoid initially resting on a planar surface [see Fig. 3(a)] in order to study rotations restricted to a plane. In this case the transition to the spinning perpendicular state is suppressed.

### 1. Mathematical model

Planar rotations are defined as $\Omega_1 = d\theta/dt$, $\Omega_2 = \Omega_3 = 0$ (i.e., around the short axis), $E_1 = 0$, $E_2 \equiv E_\perp = -E \sin\theta$, and $E_3 \equiv E_\parallel = E \cos\theta$. The polarization relaxation equations (2) reduce to

$$\frac{dP_\parallel}{dt} = -\frac{1}{\tau_\parallel}\big[P_\parallel - \big(\chi_\parallel^0 - \chi_\parallel^\infty\big)E_\parallel\big], \tag{9a}$$

$$\frac{dP_\perp}{dt} = -\frac{1}{\tau_\perp}\big[P_\perp - \big(\chi_\perp^0 - \chi_\perp^\infty\big)E_\perp\big]. \tag{9b}$$

The balance of electric and viscous torque (3) (in the inertialess limit) reduces to

$$\alpha_\perp \frac{d\theta}{dt} = P_\parallel E_\perp - P_\perp E_\parallel + \big(\chi_\parallel^\infty - \chi_\perp^\infty\big)E_\perp E_\parallel. \tag{10}$$

The time integration of the equations for the polarization evolution (9) and for the angular momentum conservation (with negligible inertia) (10) shows that the particle dynamics has three distinct stable states: spinless parallel, swinging, and tumbling [38] (see the Appendixes for more details).

### 2. Experimental results

Experiments confirm the theoretical predictions for the planar rotation. The phase diagram in Fig. 5(a) shows the regions of existence of the various states as the field strength increases: a spinless-parallel state (triangles), sustained swinging motion (square), and tumbling (circles). Unlike unbounded rotation, the distinct states are not observed to coexist.

The transient dynamics is presented in Fig. 5(b) for a particle of aspect ratio $\beta = 1.78$. Swinging is characterized by angle oscillations with constant amplitude (within $-\pi/2 < \theta < \pi/2$) for as long as the electric field is on. The amplitude can be tuned by modifying the strength of the electric field and the particle aspect ratio. Tumbling occurs when the swinging amplitude exceeds $\pi/2$. Near the threshold $E_t$ the ellipsoid might reverse its direction of rotation after a few cycles.

The experimental data are compared with the numerical solution of the set of three evolution equations describing the ellipsoid motion: the polarization (parallel and perpendicular to the applied field direction) (9) and orientation (angle between the long axis and the applied field direction) (10). Quantitative agreement for the field thresholds for swinging $E_s$ and tumbling $E_t$ [Fig. 5(a)] as well as the angle evolution [Figs. 5(c)–5(e)] is found if the conductivity of the outer fluid is
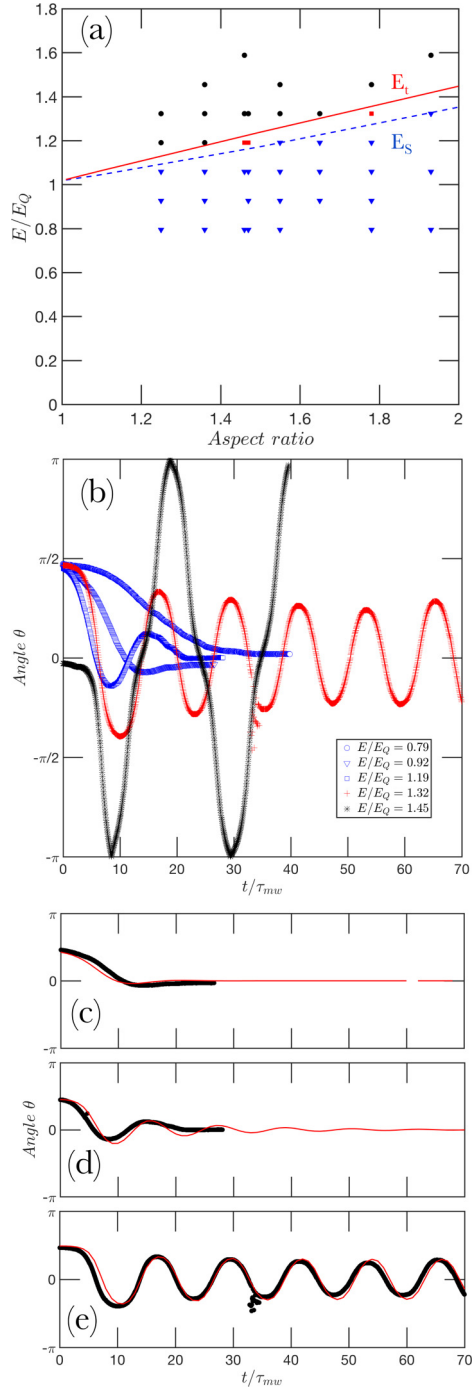
FIG. 5. (a) Phase diagram for a planar rotation: spinless parallel (triangles), swinging (squares), and tumbling (circles). Shown are the numerically obtained thresholds for swinging (blue dashed line) and tumbling (red solid line). (b) Example of transient dynamics for the ellipsoid with aspect ratio $\beta = 1.78$. Swinging (here for $-\pi/4 < \theta < \pi/4$) occurs for $E/E_Q = 1.32$ and the tumbling for $E/E_Q = 1.45$. The best numerical agreement is found for an effective conductivity of the surrounding material $0.67\sigma_s$ for (c) $E/E_Q = 0.92$, (d) $E/E_Q = 1.19$, and (e) $E/E_Q = 1.32$.

assumed to be lower by a factor of 0.67. This assumption is justified by the fact that the substrate introduces inhomogeneity in the conductivity near the ellipsoid: The insulating solid substrate with a negligible conductivity can be accounted for by an effectively lower-conductivity homogenous medium embedding the ellipsoid. Some discrepancies may still originate from the additional friction due to roughness on the particles surface and substrate.

## IV. CONCLUSION

We have investigated the electrorotation dynamics of a prolate ellipsoid under unbounded or constrained (planar) conditions. As predicted by stability analysis, the ellipsoid has the ability to either align or spin perpendicularly to the electric field. Spinning perpendicular states dominates at high electric fields and a bistability region was evidenced. Restricting the rotations from fully three dimensional to planar, by placing the ellipsoid on a surface, gives rise to dynamics such as tumbling and swinging.

This work focused on prolate ellipsoids, where rotation around the longest axis is favored due to lower friction. Oblate ellipsoids offer potentially richer behavior with the choice of rolling (spinning around the shortest, symmetry axis) or tumbling (spinning around the longer axis).

The electrorotation dynamics of ellipsoids resting on a surface offers interesting directions for research in the context of collective dynamics. The shape anisotropy adds aligning interactions, which lacks in systems of Quincke rollers [5], and this could give rise to nematic ordering.

## ACKNOWLEDGMENTS

## APPENDIX A: THEORETICAL MODEL FOR THE QUINCKE ROTATION OF AN ELLIPSOID

For the sake of completeness, here we summarize the model describing the rotational dynamics of an ellipsoid in a uniform electric field [27]. We consider a coordinate system aligned with the ellipsoid symmetry axis (and comoving with it). Charges carried by conduction accumulate at boundaries that separate media with different electric properties. The relaxation of the retarded polarization (total minus the instantaneous) along the direction of the ellipsoid axes is described by

$$\frac{dP_i}{dt} = -\frac{1}{\tau_i}\left(P_i - P_i^{\text{eq}}\right),$$ (A1)

where

$$\tau_i = \frac{\varepsilon_s}{\sigma_s}\frac{1 + n_i(S-1)}{1 + n_i(R-1)}$$ (A2)

are the Maxwell-Wagner relaxation times, with $n_i$ the depolarization factors, and $P_i^{\text{eq}}$ are the components of the equilibrium polarization, which are proportional to the components of the electric field. The coefficient of proportionality is the susceptibility

$$P_i^{eq} = \chi_i E_i,$$ (A3)

$$\chi_i = \chi_i^0 - \chi_i^\infty$$
$$= \varepsilon_s V\left[\frac{R-1}{(R-1)n_i + 1} - \frac{S-1}{(S-1)n_i + 1}\right],$$ (A4)

where $V$ is the ellipsoid volume.

For a *prolate* ellipsoid $a_3 > a_2 = a_1$ (i.e., $a_\parallel > a_\perp$), the axis of symmetry is the long axis; the aspect ratio $\beta = a_\parallel/a_\perp > 1$,

$$n_3(\equiv n_\parallel) = \frac{1-e^2}{e^3}[\text{arctanh}(e) - e],$$

$$n_1 = n_2 = \frac{1-n_3}{2}, \tag{A5}$$

where $e = \sqrt{1 - 1/\beta^2}$. The evolution of the ellipsoid orientation is determined from the conservation of angular momentum

$$I_i \frac{d\Omega_i}{dt} = (\bar{\mathbf{P}} \times \mathbf{E})_i - \alpha_i \Omega_i, \tag{A6}$$

where $I_i$ are the moments of inertia around $i$th axis and $\alpha_i$ are the friction coefficients [34]

$$\alpha_1 = 2\mu_s V M_\perp, \quad \alpha_2 = \alpha_1, \quad \alpha_3 = 2\mu_s V M_\parallel, \tag{A7}$$

with

$$M_\perp = \frac{1+\beta^2}{n_\parallel \beta^2 + \frac{1-n_\parallel}{2}}, \quad M_\parallel = \frac{2}{1-n_\parallel}. \tag{A8}$$

## APPENDIX B: INERTIALESS PLANAR ROTATIONS OF AN ELLIPSOID

The evolution equations (9) and (10) are nondimensionalized before solving. The variables are normalized by the values for a sphere

$$\tilde{t} = \frac{t}{\tau_{\text{MW}}}, \quad \tilde{P} = \frac{P}{P_c}, \tag{B1}$$

where

$$P_c = \Delta\chi_s E, \quad \chi^0 = \varepsilon_s 4\pi a^3 \frac{R-1}{R+2}, \quad \chi^\infty = \varepsilon_s 4\pi a^3 \frac{S-1}{S+2}, \tag{B2}$$

and $\Delta\chi_s = \chi^0 - \chi^\infty$ is given by (4). In dimensionless form, the torque balance (10) becomes

$$\dot{\theta} = -\frac{B}{2M_\perp}[C_1(\tilde{P}_\perp \cos\theta + \tilde{P}_\parallel \sin\theta) + C_2 \cos\theta \sin\theta], \tag{B3}$$

where

$$B = \frac{\varepsilon_s^2 E^2}{\mu_s \sigma_s}, \quad C_1 = \frac{9(R-S)}{(R+2)^2}, \quad C_2 = \left[\frac{(S-1)}{(S-1)n_\parallel + 1} - \frac{(S-1)}{(S-1)n_\perp + 1}\right]\left(\frac{S+2}{R+2}\right). \tag{B4}$$

The dimensionless polarization relaxation equations are

$$\frac{d\tilde{P}_\parallel}{d\tilde{t}} = -T_\parallel(\tilde{P}_\parallel - X_\parallel \cos\theta), \tag{B5a}$$

$$\frac{d\tilde{P}_\perp}{d\tilde{t}} = -T_\perp(\tilde{P}_\perp + X_\perp \sin\theta), \tag{B5b}$$

where

$$T_{\parallel,\perp} = \frac{\tau_{\text{MW}}}{\tau_{\parallel,\perp}} = \left(\frac{S+2}{R+2}\right)\left(\frac{(R-1)n_{\parallel,\perp} + 1}{(S-1)n_{\parallel,\perp} + 1}\right) \tag{B6}$$

and

$$X_{\parallel,\perp} = \frac{(R+2)(S+2)}{9[1+n_{\parallel,\perp}(R-1)][1+n_{\parallel,\perp}(S-1)]}.$$ (B7)

The numerical results in Fig. 5 are obtained by the time integration of (B5) and (B3).

___

[1] G. Quincke, Ueber Rotationen im constanten electrischen Felde, Ann. Phys. **295**, 417 (1896).

[2] E. Lemaire and L. Lobry, Chaotic behavior in electro-rotation, Physica A **314**, 663 (2002).

[3] F. Peters, L. Lobry, and E. Lemaire, Experimental observation of Lorenz chaos in the Quincke rotor dynamics, Chaos **15**, 013102 (2005).

[4] A. Jakli, B. Senyuk, G. X. Liao, and O. Lavrentovich, Colloidal micromotor in smectic a liquid crystal driven by DC electric field, Soft Matter **4**, 2471 (2008).

[5] A. Bricard, J.-B. Caussin, N. Desreumaux, O. Dauchot, and D. Bartolo, Emergence of macroscopic directed motion in populations of motile colloids, Nature (London) **503**, 95 (2013).

[6] H. Sato, N. Kaji, T. Mochizuki, and Y. H. Mori, Behavior of oblately deformed droplets in an immiscible dielectric liquid under a steady and uniform electric field, Phys. Fluids **18**, 127101 (2006).

[7] P. F. Salipante and P. M. Vlahovska, Electrohydrodynamics of drops in strong uniform dc electric fields, Phys. Fluids **22**, 112110 (2010).

[8] P. F. Salipante and P. M. Vlahovska, Electrohydrodynamic rotations of a viscous droplet, Phys. Rev. E **88**, 043003 (2013).

[9] M. Ouriemi and P. M. Vlahovska, Electrohydrodynamics of particle-covered drops, J. Fluid Mech. **751**, 106 (2014).

[10] M. Ouriemi and P. M. Vlahovska, Electrohydrodynamic deformation and rotation of a particle-coated drop, Langmuir **31**, 6298 (2015).

[11] P. M. Vlahovska, Electrohydrodynamic instabilities of viscous drops, Phys. Rev. Fluids **1**, 060504 (2016).

[12] B. Bharti and O. D. Velev, Assembly of reconfigurable colloidal structures by multidirectional field-induced interactions, Langmuir **31**, 7897 (2015).

[13] A. van Blaaderen, M. Dijkstra, R. van Roij, A. Imhof, M. Kamp, B. W. Kwaadgras, T. Vissers, and B. Liu, Manipulating the self assembly of colloids in electric fields, Eur. Phys. J Spec. Top. **222**, 2895 (2013).

[14] I. S. Aranson, Collective behavior in out-of-equilibrium colloidal suspensions, C. R. Phys. **14**, 518 (2013).

[15] J. Dobnikar, A. Snezhko, and A. Yethiraj, Emergent colloidal dynamics in electromagnetic fields, Soft Matter **9**, 3693 (2013).

[16] D. Das and D. Saintillan, Electrohydrodynamic interaction of spherical particles under Quincke rotation, Phys. Rev. E **87**, 043014 (2013).

[17] Y. Dolinsky and T. Elperin, Dipole interaction of the Quincke rotating particles, Phys. Rev. E **85**, 026608 (2012).

[18] E. Lushi and P. M. Vlahovska, Periodic and chaotic orbits of micro-rotors in creeping flows, J. Nonlinear Sci. **25**, 1111 (2015).

[19] A. Bricard, J.-B. Caussin, D. Das, C. Savoie, V. Chikkadi, K. Shitara, O. Chepizhko, F. Peruani, D. Saintillan, and D. Bartolo, Emergent vortices in populations of colloidal rollers, Nat. Commun. **6**, 7470 (2015).

[20] M. Belovs and A. Cēbers, Relaxation of polar order in suspensions with Quincke effect, Phys. Rev. E **89**, 052310 (2014).

[21] K. Yeo, E. Lushi, and P. M. Vlahovska, Collective Dynamics in a Binary Mixture of Hydrodynamically Coupled Microrotors, Phys. Rev. Lett. **114**, 188301 (2015).

[22] A. Cēbers, Bistability and "Negative" Viscosity for a Suspension of Insulating Particles in an Electric Field, Phys. Rev. Lett. **92**, 034501 (2004).

[23] E. Lemaire, L. Lobry, and N. Pannacci, Viscosity of an electro-rheological suspension with internal rotations, J. Rheol. **52**, 769 (2008).

[24] H.-F. Huang, M. Zahn, and E. Lemaire, Negative electrorheological responses of micro-polar fluids in the finite spin viscosity small spin velocity limit. I. Couette flow geometries, J. Electrostat. **69**, 442 (2011).

[25] N. Pannacci, E. Lemaire, and L. Lobry, DC conductivity of a suspension of insulating particles with internal rotation, Eur. Phys. J. E **28**, 411 (2009).

[26] J. R. Melcher and G. I. Taylor, Electrohydrodynamics—A review of role of interfacial shear stress, Annu. Rev. Fluid Mech. **1**, 111 (1969).

[27] A. Cēbers, E. Lemaire, and L. Lobry, Electrohydrodynamic instabilities and orientation of dielectric ellipsoids in low-conducting fluids, Phys. Rev. E **63**, 016301 (2000).

[28] T. B. Jones, Quincke rotation of spheres, IEEE Trans. Industry Appl. **IA-20**, 845 (1984).

[29] I. Turcu, Electric field induced rotation of spheres, J. Phys. A: Math. Gen. **20**, 3301 (1987).

[30] A. Cēbers, Dynamics of an elongated magnetic droplet in a rotating field, Phys. Rev. E **66**, 061402 (2002).

[31] Y. Dolinsky and T. Elperin, Equilibrium orientation of an ellipsoidal particle inside a dielectric medium with a finite electric conductivity in the external electric field, Phys. Rev. E **71**, 056611 (2005).

[32] Y. Dolinsky and T. Elperin, Dynamics of a spheroidal particle in a leaky dielectric medium in an ac electric field, Phys. Rev. E **73**, 066607 (2006).

[33] Y. Dolinsky and T. Elperin, Stability of particle rotation in a rotating electric field, Phys. Rev. E **79**, 026602 (2009).

[34] Y. Dolinsky and T. Elperin, Electrorotation of a leaky dielectric spheroid immersed in a viscous fluid, Phys. Rev. E **80**, 066607 (2009).

[35] T. B. Jones, *Electromechanics of Particles* (Cambridge University Press, New York, 1995).

[36] A. O. Tsebers, On the chaotic solution of relaxation equations of electric polarization, Magnetohydrodynamics **27**, 251 (1991).

[37] A. Cebers, Chaos in polarization relaxation of a low-conducting suspension of anisotropic particles, J. Magn. Magn. Mater. **122**, 277 (1993).

[38] A. Musial, Nonlinear electrohydrodynamics of non-spherical particles, M.S. thesis, Dartmouth College, 2011.

[39] See Supplemental Material at http://link.aps.org/supplemental/10.1103/PhysRevFluids.2.014101 for a movie.